

Near-Earth Object Astrometric Interferometry⁵

MARTIN R. WERNER

The George Washington University

Introduction

Using astrometric interferometry on near-Earth objects (NEOs) poses many interesting and difficult challenges. Poor reflectance properties and potentially no significant active emissions lead to NEOs having intrinsically low visual magnitudes. Using worst case estimates for signal reflection properties leads to NEOs having visual magnitudes of 27 and higher. Today the most sensitive interferometers in operation have limiting magnitudes of 20 or less. The main reason for this limit is due to the atmosphere, where turbulence affects the light coming from the target, limiting the sensitivity of the interferometer. In this analysis, the interferometer designs assume no atmosphere, meaning they would be placed at a location somewhere in space. Interferometer configurations and operational uncertainties are looked at in order to parameterize the requirements necessary to achieve measurements of low visual magnitude NEOs. This analysis provides a preliminary estimate of what will be required in order to take high resolution measurements of these objects using interferometry techniques.

Theory

Interferometry is the measurement of interference patterns produced by combining the light from two or more telescopes that observe the same source. The theory behind interferometry is actually quite simple: when two coherent beams of light are overlapped, the waves will interfere with each other, creating an interference pattern. If the two waves are in phase, they will combine constructively and produce an intensity that is more than twice the combination of the two separate source intensities. When the two waves are 180° out of phase, they will cancel destructively, reducing the intensity to zero. This fluctuation in the intensity as the phase is changed is measured by the interferometer and used to produce a position measurement.

Setup and Measurements

Figure 1 shows the basic setup of an interferometer. The vector between the two telescopes is known as the baseline \mathbf{B} . The vector from the centerline of the interferometer to the source being observed is called the position vector \mathbf{S} .

Because the target being observed does not usually lie on the perpendicular axis of the interferometer, the light waves from the source will reach one telescope before the other. The distance the wave must travel to reach the second telescope after reaching the first is the delay distance or D as shown in figure 1. The value of D for an interferometer is given by

$$D = \hat{\mathbf{s}} \cdot \mathbf{B} + C \quad (1)$$

where $\hat{\mathbf{s}}$ is the unit position vector, \mathbf{B} is the baseline vector, and C is a calibration term. Both $\hat{\mathbf{s}}$ and \mathbf{B} are three-dimensional vectors. The calibration term should remain constant for a given interferometer, and for simplification it is assumed to be zero. This equation can then be written in the form

$$D = |\mathbf{B}| \cos \theta \quad (2)$$

⁵Chapter nomenclature available in chapter notes, p. 217.

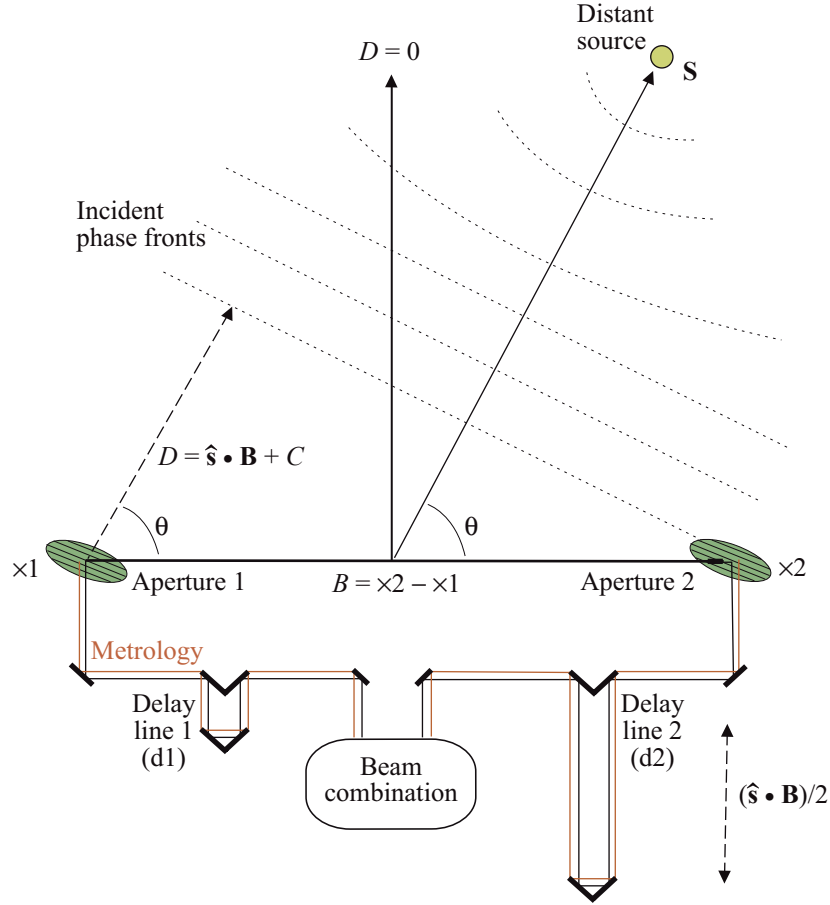


Figure 1. Basic interferometry layout.

where θ is the angle between the $\hat{\mathbf{s}}$ and \mathbf{B} vectors. The goal is to measure the baseline distance and the delay position and then solve for the target's angular position θ . The delay position is found by moving the internal delay lines until the internal delay distance equals D . As the delay line is varied, the interferometer measures an intensity pattern, which will look similar to figure 2. The internal delay is equal to D at the point of maximum fringe intensity. When this point is reached, the value of the internal delay is then measured and used to solve for θ . To find the position of the star in inertial space, the baseline vector orientation with respect to inertial space must be found. For ground-based interferometers, baseline orientation is usually done before the science measurement by first taking measurements of reference stars that have well-known positions in inertial space. This can be done reliably on the ground because the baseline is relatively stable over long time periods. For a space-based interferometer, such as the one planned for the Space Interferometry Mission (SIM) in reference 1, two guide interferometers can be used that are tied to the science interferometer at the picometer level. These guide interferometers will lock on to reference stars and measure the spacecraft's inertial position at the same time as the science measurement. This is necessary because there is no stable surface to which the interferometer can be attached, and the baseline will fluctuate over the period of science observations. A given baseline orientation will only give a one-dimensional measurement of θ . To get the actual two-dimensional target position (i.e., latitude and longitude), two measurements will need to be taken using orthogonal baselines.

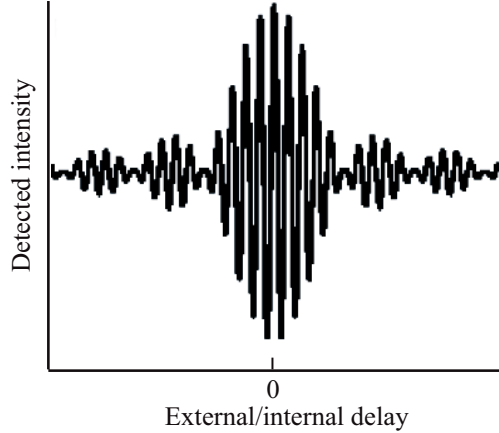


Figure 2. Interferometric intensity pattern.

Resolution

The preliminary requirement for a Comet/Asteroid Protection System (CAPS) astrometric interferometer is to achieve angular position accuracy (σ_θ) of 100 microarcseconds (μas), which can also be referred to as the resolution. Therefore, an error taken in the angular measurement will be off by no more than 100 μas . To achieve this resolution, the delay position and baseline distance must be measured with an accuracy of at least 1 nm (ref. 2). Distance measurements can be done using laser metrology systems that are already being used in ground-based interferometers. Measuring the delay position will not be the problem. The problem is getting the internal delay mirror in the correct place to produce the maximum fringe intensity because this value of delay corresponds to the actual angle. It is necessary to establish how accurately the position of the central fringe can be determined. Accuracy that the interferometer can achieve in detecting the central fringe can be estimated using

$$\sigma_\theta \approx \frac{\lambda/B}{\text{SNR}} \quad (3)$$

where λ is the average wavelength in micrometers, B is the baseline in meters, and SNR is the signal-to-noise ratio. The top part of the equation gives the width of the fringes that are produced. The smaller the width of the fringe, the easier it is to pick out from an adjacent fringe. Increasing the baseline decreases the fringe width, improving the resolution of the interferometer. Furthermore, an interferometer has the ability to improve on this resolution depending on the SNR. As the SNR is increased, the interferometer can better pinpoint the exact center of the fringe, resulting in a higher accuracy measurement. This improvement in accuracy is analogous to blur centroiding with a single aperture telescope where the centroid position of the star can be measured to much less than the size of the airy disk (ref. 3). It must be noted that this equation is only an approximation and will ultimately depend on the detection system and tracking algorithms used.

Fringe Visibility

Fringe visibility (V) is the apparent contrast between light and dark areas of the fringe pattern and is defined by

$$V = \frac{I_{\text{MAX}} - I_{\text{MIN}}}{I_{\text{MAX}} + I_{\text{MIN}}} \quad (4)$$

where V is a dimensionless value contained on the interval $[0,1]$, I_{MAX} is the maximum fringe intensity, and I_{MIN} is the minimum fringe intensity (ref. 4). There are many factors that will affect the fringe visibility. With strict interferometer design, construction, and operation, most of the factors can be taken out. However, one factor that must be considered for observations of near-Earth objects (NEOs) is the visibility loss caused by overresolving the target. Ideally, the target object should be a point source; however, an NEO in the solar system is potentially close enough such that it is no longer a point source, but instead is a uniform disk. When looking at a uniform disk, each point on the disk will create its own fringe pattern that will overlap the other fringe patterns. As the baseline gets longer, the more the fringes overlap, blurring out the ideal fringe pattern. Overresolving reduces the fringe visibility, reducing the amplitude of the intensity peaks, making the fringes harder to pick out from one another above the noise and ultimately reducing the measurement accuracy. This visibility effect is given by

$$V = \frac{2J_1(\pi B\theta_{ud}/\lambda)}{(\pi B\theta_{ud}/\lambda)} \quad (5)$$

where θ_{ud} is the width of the uniform disk measured at the detector in radians (rad), and J_1 is the first order Bessel function (ref. 5). Referred to as the “target width” throughout the rest of this analysis, θ_{ud} is calculated using

$$\theta_{ud} = \tan^{-1}\left(\frac{d}{x_{det}}\right) \quad (6)$$

where d is the diameter of the target and x_{det} is its distance from the detector (assuming that $x_{det} \gg d$). The target width will affect fringe visibility and place limitations on the length of baseline that can be used.

Dwell Time

Dwell time (T) is the amount of time that can be spent at a single delay position, before uncertainty overwhelms the measurement, and is defined by

$$T \leq \frac{c/\delta\nu}{\sigma\dot{D}} \quad (7)$$

where c is the speed of light, $\delta\nu$ is the bandwidth, and $\sigma\dot{D}$ is the delay rate uncertainty (ref. 6). The maximum dwell time depends on uncertainties in the motions of the interferometer and of the target, which affect the delay rate uncertainty. Uncertainties in the delay rate will cause the fringes to move on the detector, so the dwell time must be short enough that the intensity measurement can be taken before the desired fringe moves off the detector.

Photon Rate

To successfully take a measurement of an NEO, a certain amount of signal in a given amount of time is needed. There are many factors that affect the signal that reaches the detector. The goal is to determine how many photons per second are being collected by the interferometer. In this analysis, the photon rate (R) at the detector is found using

$$R = R_0 \cdot 2.512^{-M} \cdot \frac{\pi}{4} D_T \cdot \eta \cdot \delta\nu \quad (8)$$

where R_0 is the zero visual magnitude photon rate, M is the visual magnitude of the NEO, D_T is the diameter of the collecting aperture, η is the throughput efficiency of the interferometer, and $\delta\nu$ is the instrument bandwidth.

Signal-to-Noise Ratio

SNR, by definition, is the ratio of total signal received to the noise. The SNR is estimated using

$$\text{SNR} \approx \frac{R \cdot T \cdot V}{\sqrt{R \cdot T + 4 \frac{V}{\delta\nu} r^2}} \quad (9)$$

The numerator of equation (9) is the total amount of signal received by the interferometer and is affected by the photon rate, dwell time, and visibility. The denominator is the total amount of noise, which includes photon noise and read noise. Possible noise caused by background sources was excluded from this analysis and needs to be studied and accounted for in future analysis. Background noise, if present, will lower the SNR for a given measurement, increasing the requirement on telescope diameter or dwell time to complete a successful measurement. Photon noise is due to the nature of light. The actual rate of photons received from the target object will fluctuate over time, giving a natural fluctuation in the intensity that affects the measurement of the fringes. The standard deviation of the photon noise is given by \sqrt{N} , where N is the total number of photons collected in a given time. Read noise is a property of the detector and is due to random energy being picked up by the detector and recorded as photons during each pixel readout. The read noise has a standard deviation (r), which results in a variance in each read of r^2 . For each fringe measurement, the detector should read out four times. The total number of fringes in the fringe pattern is approximated by taking the average wavelength over the bandwidth of the interferometer (ref. 1). Multiplying these three terms together gives the total read noise. Both the photon noise and read noise are added together, and the square root of that number gives the total noise for each measurement. Detectors are being developed that suggest subelectron read noise errors will be possible (ref. 7), essentially eliminating the effects of read noise. However, read noise is still included in this analysis to place an upper bound on the results.

Assumptions

Many different factors can be looked at for interferometry calculations. For simplification, multiple assumptions are made about the interferometer setup in this analysis. This section includes the assumptions used for the calculations that are performed.

Observing Conditions and Location

The main assumption of a CAPS-based interferometer is that it is placed in a location absent of atmosphere. The atmosphere is the largest source of error that limits Earth-based interferometers. Turbulence in the atmosphere places great restrictions on the signal and maximum dwell time that can be achieved. The limitations on dwell time alone would make the telescope size requirements impractical for a system designed to view such low magnitude objects. Two possibilities for an interferometer location could be either in a heliocentric orbit around the Sun or on the Moon. The advantages and disadvantages are briefly discussed for both these locations subsequently; however, for this analysis, no specific location is defined. The only thing specific about the detector location is that it is positioned at a distance of 1 astronomical unit (au) from the Sun.

Heliocentric orbit. At a location 1 au from the Sun, the detector could be placed in an Earth leading or trailing orbit. An advantage of this orbit is that the interferometer could theoretically be aimed in any direction. However, this also can be a disadvantage because of the fuel requirements and vibrations introduced during the maneuver. Keeping a stable platform is also a problem at this location. All vibrations must be actively controlled or passively damped. Thermal issues are a concern as well because the spacecraft will always be in sunlight.

Moon. Placing an interferometer on the Moon would be very similar to an Earth-based interferometer. Having the hardware fixed to the lunar surface keeps the baseline very stable. Additionally, thermal variations could be minimized during lunar night or by locating the interferometer in a crater that offers significant shadowing. Disadvantages of lunar-based interferometers include the problem of lunar dust degrading the optics, and observations are constrained by the Moon's rotation rate and the detector's geographic location.

Control and Measurement Accuracy

The interferometer is assumed to have metrology systems that achieve 1 nm accuracy in delay and baseline distance measurements. The only error that is assumed to be present in the CAPS interferometer is the delay rate uncertainty. Also, the only fringe visibility loss present is that due to the baseline length and target width parameter discussed previously. All other visibility losses are assumed to be negligible and not included in the calculations.

Interferometer Configuration

This analysis assumes that the interferometer is using a pupil plane configuration with a single pixel charge-coupled device (CCD) type detector. The throughput efficiency is assumed to be 80 percent and includes losses due to imperfections in the optics and the quantum efficiency of the detector. This value of throughput efficiency is very high, and superior design of the interferometer and improvements in detectors are needed to produce a throughput efficiency of this value. Advancements in the next 25 years should allow this value to be obtained and makes it a reasonable estimate for this simulation. The interferometer is assumed to have a bandwidth from 500 to 1000 nm (3.0×10^{14} to 6.0×10^{14} Hz), which results in an average wavelength of 750 nm (4.0×10^{14} Hz). The read noise of the detector is assumed to be 3 electrons per read.

Analysis Cases

Four cases were analyzed consisting of an impacting long-period comet trajectory with four different initial observation distances. The CAPS detection scenario defines that interferometry, or another method that can achieve 100 μ as resolution, will be used once the impacting orbit has been refined such that the mean erroneous predicted miss distance ϵ is less than 1 lunar distance. Therefore, the object will have traveled some distance closer to the Sun between the time when it is first observed and when ϵ is found to be 1 lunar distance. This new distance is referred to as the "watch distance." Once the NEO reaches the watch distance, the orbit determination using the single 10-milliarcsecond (mas) resolution telescope will have an estimated trajectory of the object. The trajectory will have uncertainties in its angular rate. Values for the watch time and angular rate uncertainty were provided by the orbit determination analysis, and averages were taken of these values and listed in table 1. The four analysis cases will be defined by their respective watch distances. Figure 3 shows a plot of the angular rate uncertainties versus watch distance for each analysis case. The farther an object is away from the Sun, the higher its angular rate error will be when it reaches the watch distance.

Table 1. Analysis Case Initial Rate Uncertainty

Start distance, au	Watch distance, au	Rate uncertainty, rad/s	
		Longitude	Latitude
5	4.69	2.42745×10^{-13}	9.15576×10^{-13}
7	6.73	4.18491×10^{-13}	1.01544×10^{-12}
9	8.78	1.40205×10^{-12}	1.65268×10^{-12}
11	10.79	1.80448×10^{-12}	1.92439×10^{-12}

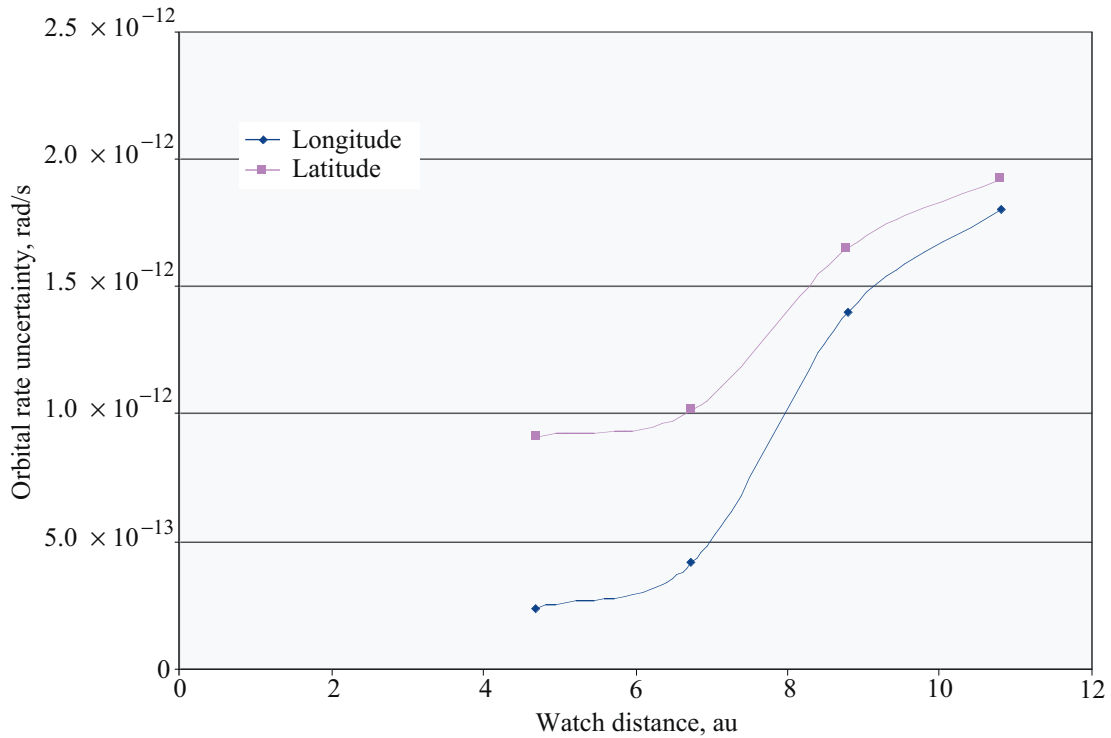


Figure 3. Average orbital rate uncertainty versus watch distance.

NEO Properties

For all four analysis cases, the NEO is assumed to be a 1-km diameter, spherical object. The value chosen for the albedo is 0.02. This value is estimated as the lowest albedo that will be encountered and is used for worst case analysis. If the detection system is designed to observe objects with this albedo at a given distance and diameter, it will be able to detect the entire range of objects at this size and distance.

Default Values

Table 2 includes the default parameter values and constants used in this analysis. These values are used for all calculations unless otherwise specified.

Table 2. Default Parameters and Constants for Analysis

Parameter	Value	Units
Target diameter	1000	meters
Target albedo	0.02	
Desired resolution	0.0001	arcsec
Average wavelength	750	nm
Instrument bandwidth	4.0×10^{14}	Hz
	500–1000	nm
Throughput efficiency	3.0×10^{14}	Hz
	0.8	
Read noise (std. dev.)	3	electrons
Speed of light	2.99792458×10^8	m/s
Magnitude zero photon rate	1.0×10^{-4}	photons/s/m ² /Hz

Signal Properties of NEOs

To obtain visual magnitude estimates, an algorithm by Basil H. Rowe was used (ref. 8). The algorithm was modified to output the visual magnitude given an NEO’s diameter. As previously mentioned, the detector distance from the Sun is assumed to be 1 au. The value used for the photometric slope was 0.15. Using the modified algorithm, a visual magnitude contour plot was created that shows the values of visual magnitude as a function of distance and direction from the Sun and the detector (fig. 4). The blue circles represent the watch distance for each analysis case. Therefore, depending on the detector location, the NEO can have any visual magnitude that the blue lines pass through.

To determine the actual range of visual magnitudes that will be expected, the Sun angle θ_S is introduced to specify where the NEO is with respect to the Sun and detector. Shown in figure 5 are the geometry of the Sun, the detector, and the definition of the Sun angle. A Sun angle of 180° is defined as that point when the detector is located directly between the Sun and the NEO; whereas, a Sun angle of 0° is when the detector is located on the opposite side of the Sun. Due to symmetry, it is not necessary to go higher than 180° .

Using this configuration, a plot of Sun angle versus visual magnitude was made and is shown in figure 6. The brightest visual magnitude is when the Sun angle is 180° . The Sun angle that gives the dimmest visual magnitude changes with the object distance from the Sun. As the object gets farther away, the Sun angle that gives the worst visual magnitude increases toward 90° . For the four analysis cases, the values of the Sun angle that produce the lowest visual magnitude range from 48° to 55° and are listed on figure 6.

Best and worst case scenarios are defined for each analysis case using the brightest and dimmest visual magnitudes and their respective Sun angles. These values are summarized in table 3. As a general rule-of-thumb, for each analysis case, as the distance is increased by 2 au, the visual magnitude drops by approximately 1 magnitude.

Visual magnitude for 1-km NEO: albedo = 0.02,
reference circle = 4.69, 6.73, 8.78, and 10.79 au

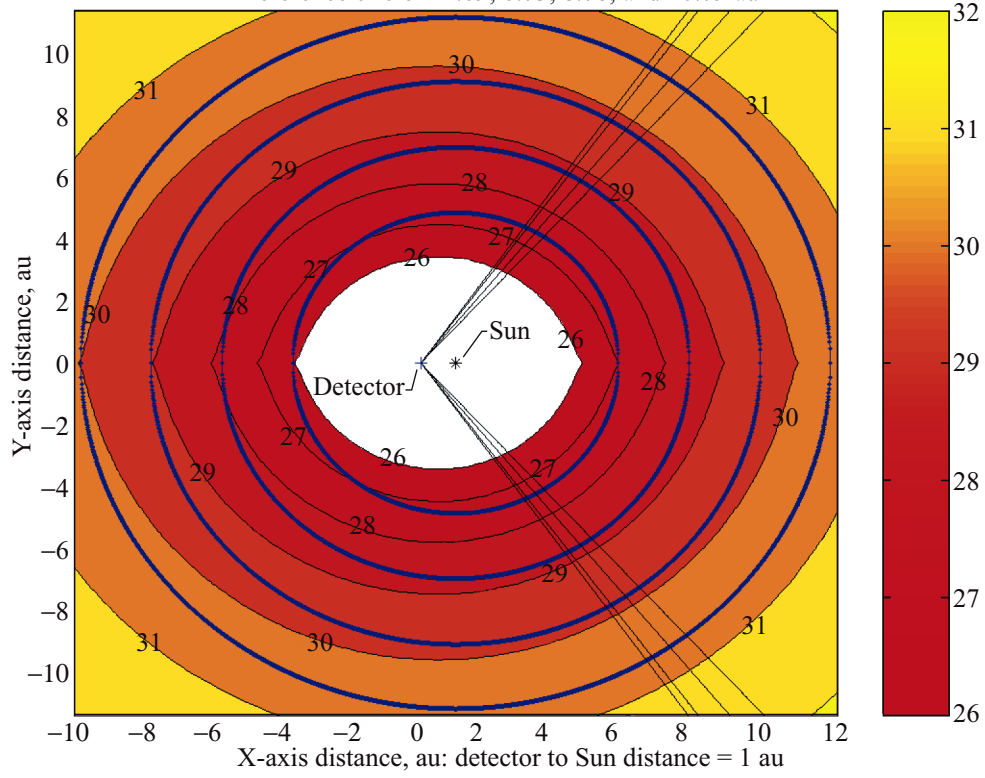


Figure 4. Visual magnitude contour plot for 1-km-diameter NEO.

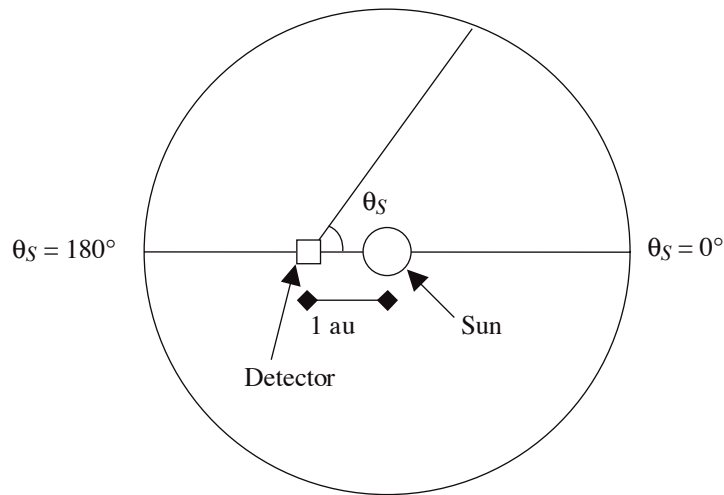


Figure 5. Sun angle geometry.

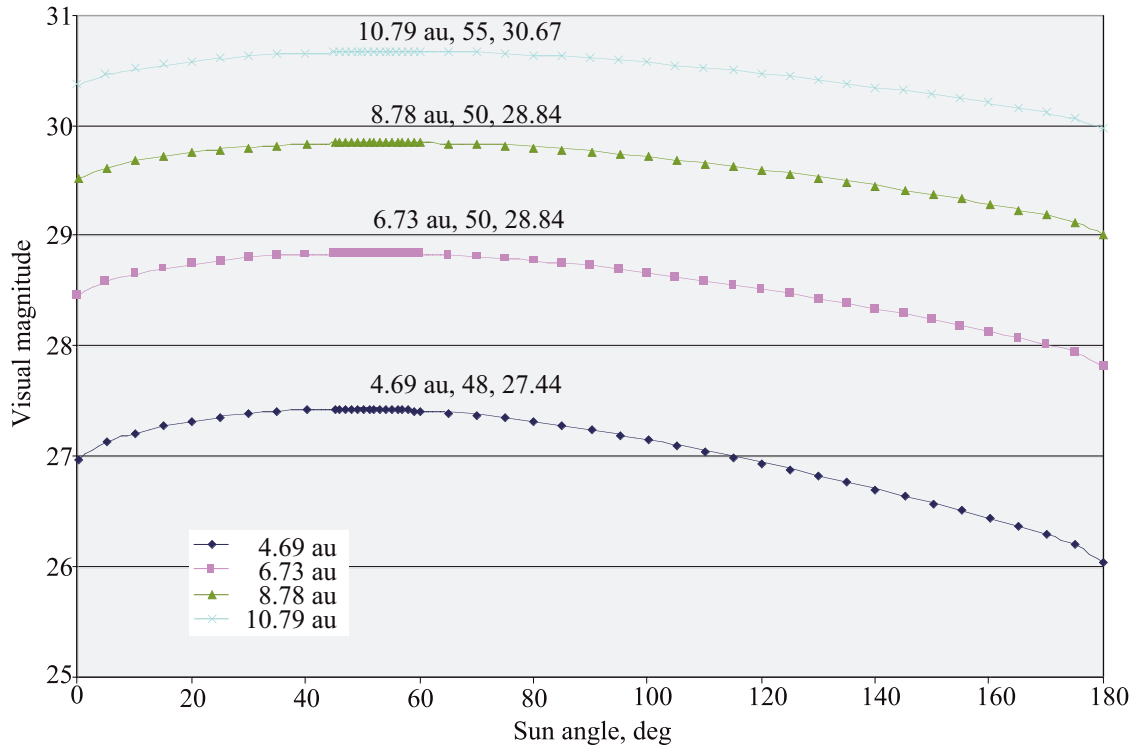


Figure 6. Visual magnitude versus Sun angle.

Table 3. Visual Magnitude Ranges Using Worst Case Albedo

Watch distance, au	4.69	6.73	8.78	10.79
Best scenario visual magnitude	26.04	27.78	29.02	29.97
Worst scenario visual magnitude/Sun angle, deg	27.44/48	28.84/51	29.85/54	30.67/55

Observing Considerations

Before final analysis can be performed, value ranges and limitations for different interferometer parameters and configurations must be looked at.

SNR, Baseline Length, and Visibility

From equation (3), in order to achieve the desired resolution of $100 \mu\text{s}$, there needs to be a certain SNR for each baseline in order to achieve this accuracy. Using the mean wavelength value of 750 nm , baseline length versus the required SNR to achieve a resolution of $100 \mu\text{s}$ is plotted in figure 7.

Figure 7 shows that as the baseline is increased, the SNR required to achieve the desired resolution gets smaller. From this plot alone it would appear that using an extremely large baseline would be ideal for keeping the necessary photon rate to a minimum; however, there is a limitation to the maximum

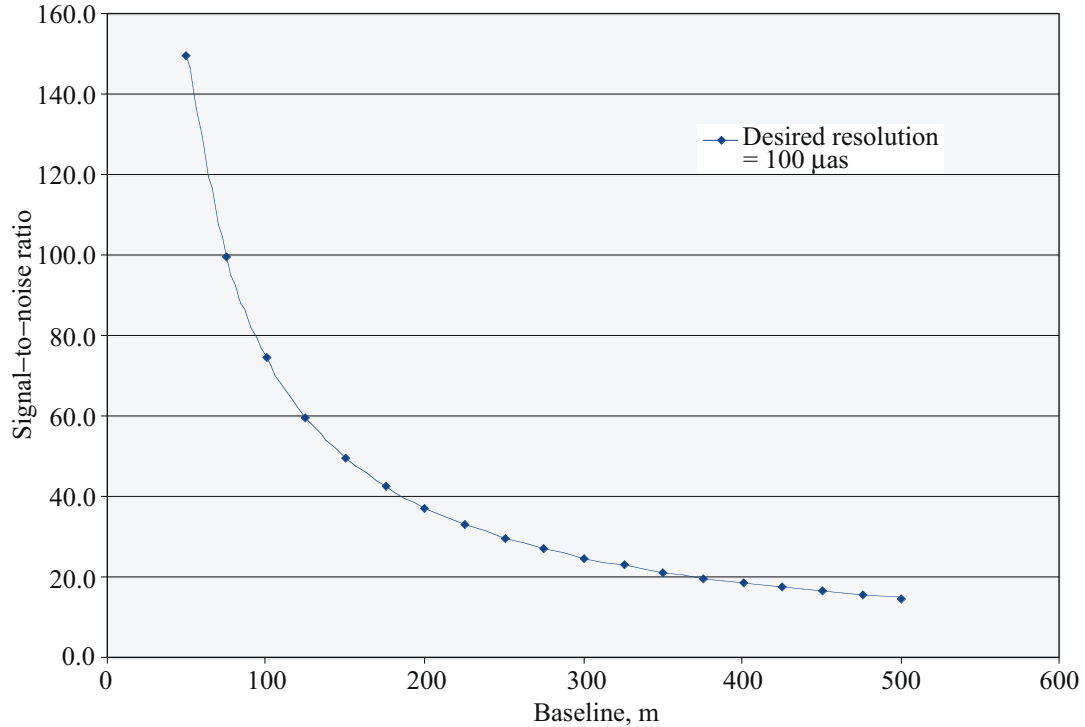


Figure 7. SNR requirement for given baseline length.

baseline that can be used for observing the desired targets. Increasing the baseline overresolves the target object, causing the fringe visibility to drop. If the baseline is increased too far, the fringe visibility will drop to zero and no interference fringes will be produced. Using equation (5) and the value the target diameter associated with the best scenario for each of the four cases, a plot of fringe visibility versus baseline length is made and shown in figure 8.

In figure 8, as the target width increases, increasing the baseline length causes the fringe visibility to drop off faster. This means for larger width objects, a smaller baseline must be used to produce the same visibility as a smaller width object with a longer baseline. In other words, the farther the object is away from the detector, the smaller its diameter will be, allowing a longer baseline to produce the same visibility.

Simulation Results

Increasing the baseline reduces the SNR required to achieve 100- μm accuracy, but it also decreases the fringe visibility, which in turn reduces the amount of signal. Therefore, a comparison of these two properties was considered to see if an optimum baseline exists that balances the required SNR and fringe visibility. This was done by taking equation (9) and solving for R , then substituting in equations (3) and (5) for the SNR and V , respectively. The required photon rate to achieve 100- μm measurements is graphed versus baseline length and is shown in figure 9.

Figure 9 clearly shows that for each case there is an optimal baseline length giving the lowest photon rate requirement. Detailed analysis at these optimal points results in a constant value of the fringe visibility for each case of approximately 0.63205. Because V is constant, the only factor that affects the optimal

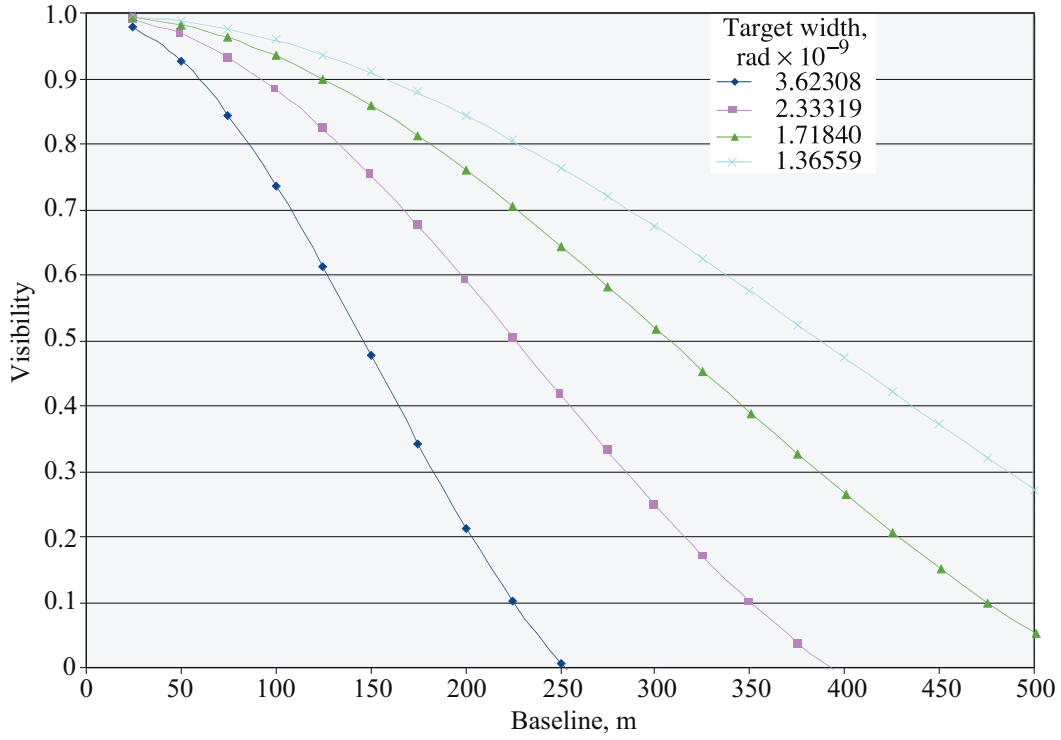


Figure 8. Effect of baseline on fringe visibility.

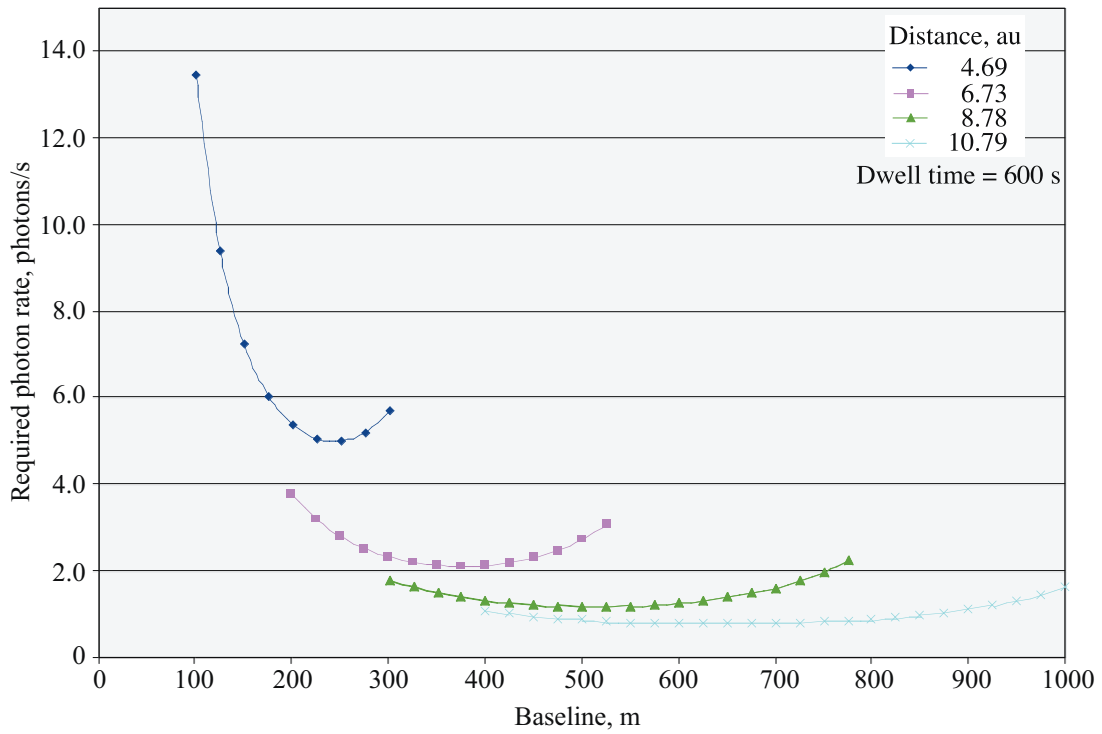


Figure 9. Effect of baseline on required photon rate.

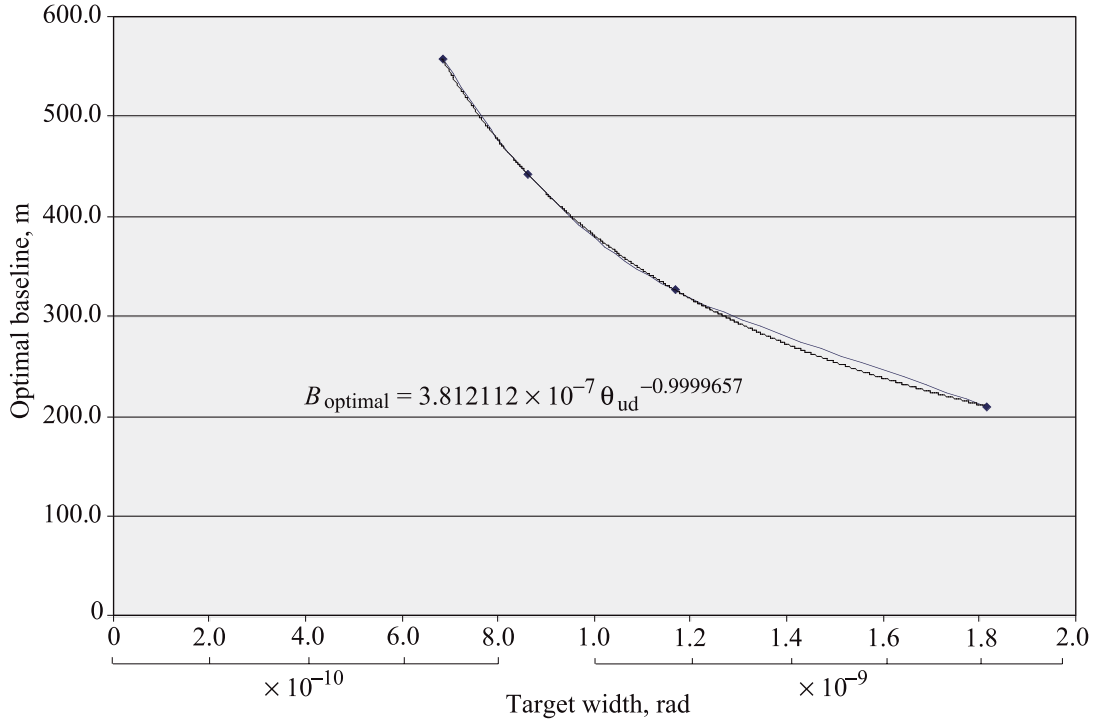


Figure 10. Optimal baseline versus target width.

baseline length is the object’s diameter and distance from the detector, which changes the target width at the telescope. Therefore, a plot of the optimal baseline versus target width was made and shown in figure 10. A power series line of best fit was performed on the data points and is given by

$$B_{\text{optimal}} = 3.812112 \times 10^{-7} \theta_{\text{ud}}^{-0.9999657} \quad (10)$$

Equation (10) can be used to estimate the optimal baseline for any object diameter and distance from the detector.

For each analysis case, upper and lower bounds are set based on the best and worst case visual magnitudes. Using the detector distances at the best and worst scenario positions of each analysis case, the optimal baseline is found and listed in table 4.

Table 4. Optimal Baselines: Best and Worst Scenarios

Watch distance, au	Best case			Worst case		
	Distance from detector, au	Target width, rad	Optimal baseline, m	Distance from detector, au	Target width, rad	Optimal baseline, m
4.69	3.69	1.81×10^{-9}	210.3	5.30	1.26×10^{-9}	302.0
6.73	5.73	1.17×10^{-9}	326.5	7.36	9.14×10^{-10}	416.6
8.78	7.78	8.59×10^{-10}	443.4	9.42	7.17×10^{-10}	531.1
10.79	9.79	6.83×10^{-10}	557.9	11.43	5.90×10^{-10}	645.7

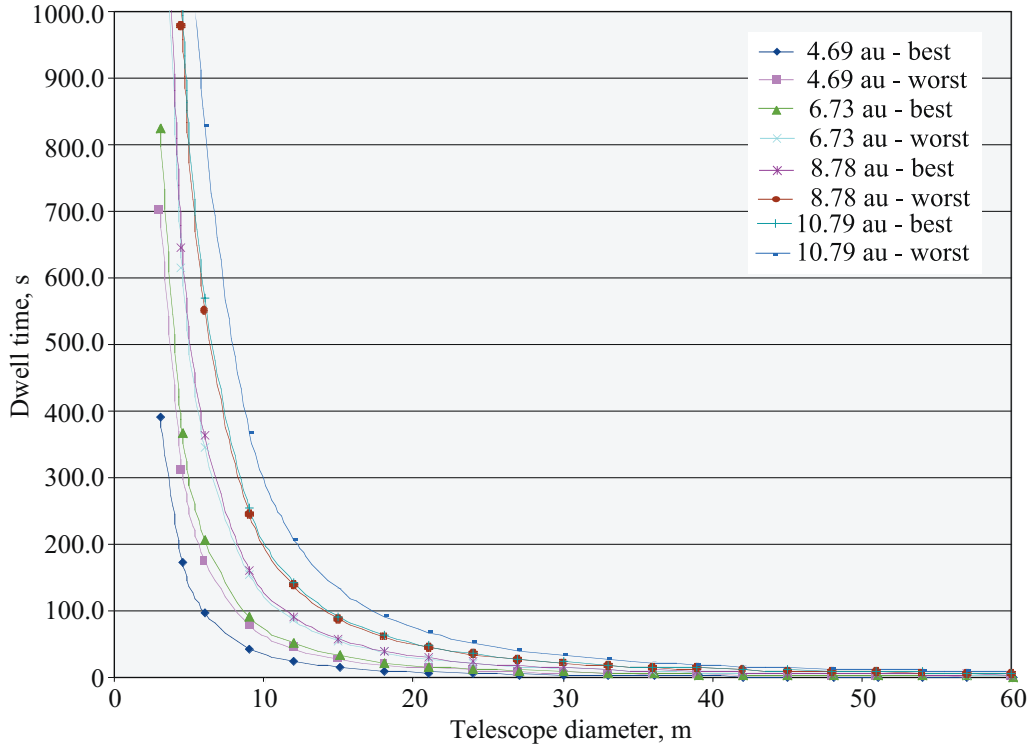


Figure 11. Dwell time and telescope size using optimal baselines.

As the optimal baseline gets longer, the SNR requirement to achieve the desired resolution goes down. Using these optimal baselines, a comparison between telescope diameter and the required dwell time needed to achieve the necessary SNR was made for each analysis case and is shown in figure 11. A study of figure 11 shows that as the telescope diameter is increased, the dwell time to achieve the necessary SNR goes down. A telescope diameter of approximately 5.5 m is sufficient to keep the dwell time requirements below 1000 s.

Telescope size will ultimately be determined by the maximum allowable dwell time that can be achieved. Referring back to equation (7), the bandwidth and speed of light will be constant. The parameter that can vary is the delay rate uncertainty. Delay rate uncertainty is caused by two effects, the angular rate error in the orbit of the NEO and the uncertainty in the motion of the interferometer. The range of possible delay rate uncertainties and the corresponding maximum allowable dwell time are listed in table 5.

If the interferometer was perfectly stable, the angular rate uncertainty would be the only factor affecting the delay rate uncertainty. The delay rate uncertainty can be found by multiplying the angular rate uncertainty by the length of half the baseline. Using the angular rate uncertainty of the worst case orbit (10.79 au = 1.92439×10^{-12} rad/s) leads to a delay rate uncertainty of approximately 1.0×10^{-9} m/s, which leads to a maximum dwell time of approximately 1000 s. Therefore, the effects of the angular motion of the NEO can be a factor when taking measurements. It is unknown how this angular uncertainty compares with that found in a space-based interferometer baseline. Once the SIM is launched in a few years, reliable data on space platform performance will be available. Until then only estimates can be made. For a lunar-based interferometer, uncertainty rates from existing Earth-based interferometers can

Table 5. Maximum Dwell Time Given Delay Rate Uncertainty

Delay rate uncertainty, m/s	Maximum dwell time, s
1.00×10^{-13}	9993082
5.00×10^{-13}	1998616
1.00×10^{-12}	999308
5.00×10^{-12}	199862
1.00×10^{-11}	99931
5.00×10^{-11}	19986
1.00×10^{-10}	9993
5.00×10^{-10}	1999
1.00×10^{-9}	999
5.00×10^{-9}	200
1.00×10^{-8}	100
5.00×10^{-8}	20
1.00×10^{-7}	10
5.00×10^{-7}	2

Table 6. Telescope Diameter Required for Given Dwell Time (Optimal Baseline)

Dwell time, s	Watch distance, au							
	4.69		6.73		8.78		10.79	
	Best, m	Worst, m	Best, m	Worst, m	Best, m	Worst, m	Best, m	Worst, m
2	42.0	56.2	61.0	78.8	80.8	100.3	101.4	122.8
10	18.8	25.1	27.3	35.3	36.1	44.8	45.3	54.9
20	13.3	17.8	19.3	24.9	25.6	31.7	32.1	38.8
100	5.9	7.9	8.6	11.1	11.4	14.2	14.3	17.4
200	4.2	5.6	6.1	7.9	8.1	10.0	10.1	12.3
999	1.9	2.5	2.7	3.5	3.6	4.5	4.5	5.5

be used as a close approximation. Because precise values of baseline angular uncertainties are not yet known, estimates for the possible delay rates that might be achieved in space are assumed to be the six largest values of delay rate uncertainty taken from table 5. Incorporated in table 6 are these values and the telescope diameter required to enable the desired astrometric accuracy in the given dwell time. Analysis of the data in table 6 shows that the dwell time plays a significant factor in the final design of an interferometer. If the delay rate uncertainty cannot be kept to less than 5.00×10^{-9} m/s, the required telescope sizes become impractical for a space-based system. Ideally, the telescope size used will be as large as possible but it will ultimately depend on the cost and size limitations and the technology available to put them into space. An ideal value to achieve in delay rate uncertainty would be around 1.0×10^{-9} m/s. This value would allow a telescope with a diameter of 6 m to take measurements in all four cases regardless of Sun angle.

To investigate the effects of using a fixed baseline, the data in figure 12 show the same results using a baseline of 150 m for each analysis case. The data in figure 12 demonstrate that using a fixed baseline

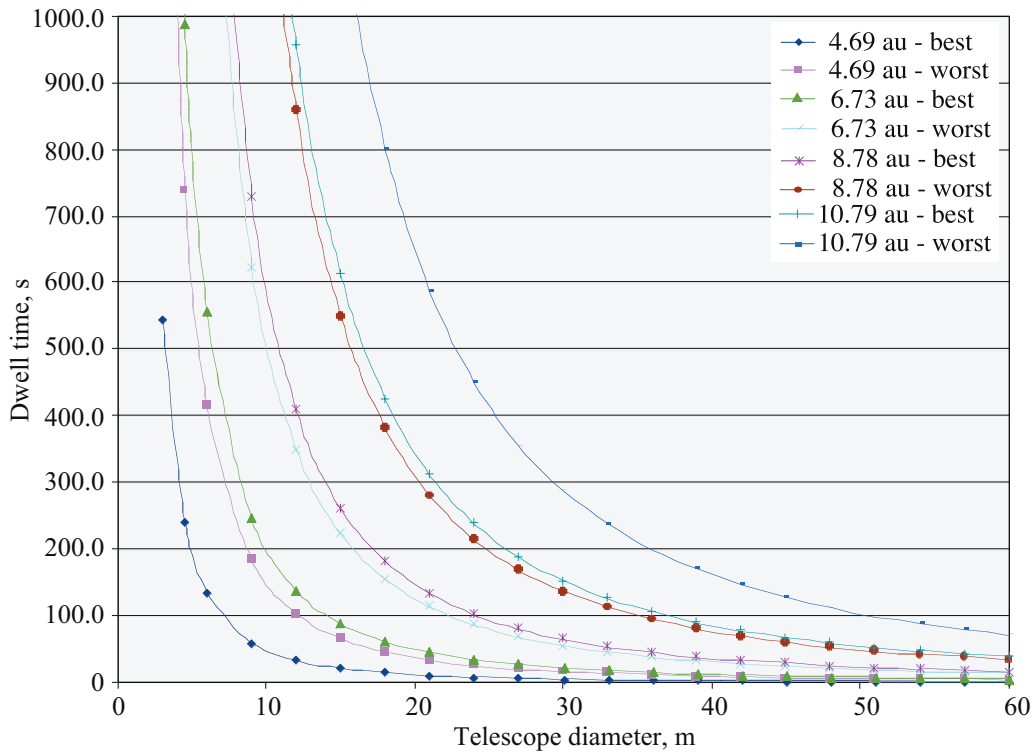


Figure 12. Dwell time and telescope size using constant baseline of 150 m.

will increase the necessary dwell time significantly, for a given telescope diameter, over a variable baseline that can be optimized. To highlight the differences in necessary dwell time, a 6-m-diameter telescope is chosen, and the respective dwell time for each case is listed in table 7. For the 150-m fixed baseline, a telescope almost three times larger (≈ 16 m) would be needed to keep the dwell time below 1000 s. The percent difference in dwell time between the optimal and fixed baseline is the same for each case regardless of the telescope diameter used.

Even with this limited set of analysis cases, there is a significant difference when an optimal baseline is used compared with a fixed baseline. The fixed baseline will be optimized for only a small range of

Table 7. Dwell Time Comparison Using 6-m-Diameter Telescope

Sun distance/case, au	Optimal baseline	150-m baseline	Difference, percent
	Dwell time, s	Dwell time, s	
4.69 - best	97.82	135.95	39.0
4.69 - worst	175.45	415.83	137.0
6.73 - best	206.53	555.89	169.2
6.73 - worst	345.26	1399.55	305.4
8.78 - best	362.7	1637.92	351.6
8.78 - worst	550.99	3438.11	524.0
10.79 - best	570.67	3825.93	570.4
10.79 - worst	828.77	7202.54	769.1

objects. For example, the fixed 150-m baseline is near the optimized baseline length for the 4.69 au range, giving only a small percent difference in dwell time. However, as the object gets farther away, the dwell time required to take the measurement using the fixed 150-m baseline increases rapidly compared with using the optimal baseline. To take a measurement of the 10.79-au object, the necessary dwell time increases by almost 800 percent. If the fixed baseline was longer, to give the best performance in the range of 10.79 au, the close objects would be overresolved and could not be measured at all. Therefore, a changeable baseline is recommended for a CAPS interferometry system. If a fixed baseline is used, it will either restrict the viewing of NEOs closer than a certain distance or place tremendous requirements on the telescope size or control accuracy in order to measure those objects farther away.

Adaptability for Small NEOs Near the Interferometer

If a system is designed that can take measurements of the four analysis cases, how will it perform on smaller sized objects? In figure 13, a visual magnitude contour plot for a 50-m NEO at distances of 0.8 and 1.2 au from the Sun is shown.

In table 8, the properties of the 1.2-au case are listed; the 0.8-au case is kept separate because the Sun angle definition breaks down once the NEO is less than 1 au from the Sun. Evaluating the numbers in table 8 shows that the CAPS interferometer would have no problem observing the 50-m object. For the best case, the visual magnitude is almost 3 magnitudes brighter than the best 4.69-au analysis case. Also, the optimal baseline is slightly larger. Observing the 50-m NEO at this location should actually be much

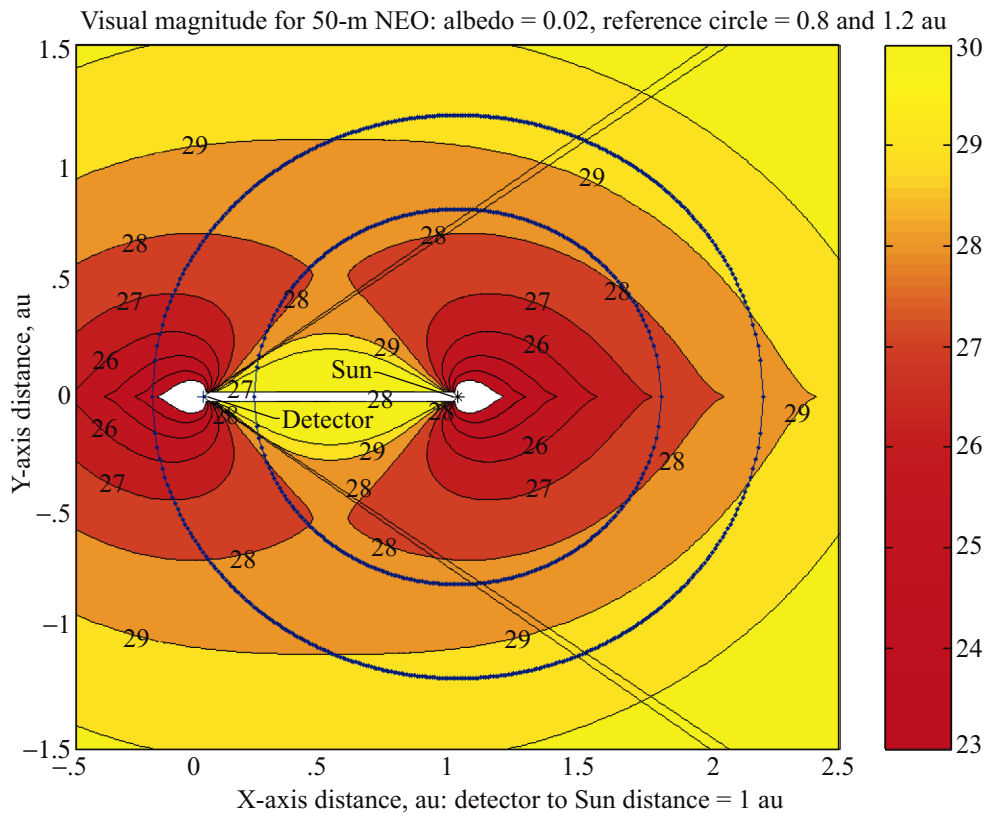


Figure 13. Visual magnitude contour for 50-m-diameter NEO.

Table 8. Detection Properties of 50-m NEO With 1.2-au Watch Distance

	Visual magnitude	Sun angle, deg	Distance from detector, au	Target width, rad	Optimal baseline, m
Best case	23.25	180	0.2	1.67115×10^{-9}	228.0
Worst case	29.37	37	1.837	1.81943×10^{-10}	2093.6

easier than any of the analysis cases. At the worst case position, the visual magnitude is comparable with that of the best 10.79-au analysis case. However, the optimal baseline is substantially larger, which would reduce the necessary photon rate to achieve the desired accuracy. Even if the baseline could only be extended to the distance of the longest analysis case, 645.7 m, the interferometer should still receive adequate signal to take the 100- μ s measurement. If the NEO is 0.8 au from the Sun, the definition of the Sun angle is no longer valid because there are two possible locations of the NEO for each Sun angle. For most of the locations in the orbit, the visual magnitude varies between 27 and 29. When the NEO starts to come between the detector and the Sun, the visual magnitude increases rapidly, essentially going to infinity when the NEO is directly between the two.

Assuming that the interferometer can view the NEO during other parts of its orbit, the interferometer should be able to take a measurement for the majority of these locations using the same reasons defined for the 1.2-au object. The actual range of NEOs that can be observed in orbits less than 1 au from the Sun will ultimately depend on the pointing restrictions of the interferometer toward the Sun. One problem might arise in viewing these 50-m objects: their initial input errors might be considerably higher than the 1-km objects due to the fact that they are moving a lot faster relative to the detector. This factor may lead to higher angular rate uncertainties and smaller maximum dwell times.

Concluding Remarks

Acquiring space-based astrometric measurements of faint near-Earth objects (NEOs) using interferometry is a formidable task. Stable interferometers with very accurate measuring systems are needed to produce the delay rate uncertainty that will lead to feasible telescope sizes. Using the desired value of 1.0×10^{-9} m/s for the delay rate uncertainty still requires telescopes approximately 6 m in diameter. Six-meter telescopes would be a good starting point for a space-based interferometer because they, as well as larger diameter telescopes, have already been built for ground-based interferometers. The next challenge is figuring out how to deploy and operate interferometers in space. Advances in technology should allow this to be possible in the foreseeable future, and even larger telescopes might be available 25 years from now. All the results in this analysis assumed the worst case for most estimates, especially the NEO albedo. Realistically, most of the NEOs that will be encountered will have a higher value of visual magnitude than used in this analysis. If the system is designed with a variable baseline, the range of objects that can be observed will be quite large.

Future Work

All calculations performed in this analysis are only first order approximations. For a more detailed analysis, specific interferometer control systems, detectors, and scanning and tracking algorithms should be used to generate more robust equations. Also, many possible sources of error were assumed to be zero for this analysis. Real life values for these errors need to be determined and used, especially values for background noise. The effects of changing the default values (like using a larger bandwidth) of the interferometer should be studied. Location will play a big role in the errors produced by the interferometer. Specific locations need to be determined and estimated errors need to be calculated at those locations.

There are some space-based interferometry technology demonstrator missions, including the Space Interferometry Mission, planned for the near future that should provide more information regarding this problem.

References

1. Halverson, P. G., et al.: Progress Towards Picometer Accuracy Laser Metrology for the Space Interferometry Mission. *International Conference of Space Optics*, ISCO 2000, Dec. 5–7, 2000, Toulouse, France.
2. Boden, A.: Interferometric Narrow-Angle Astrometry: Data Analysis. Slides from the 2001 Michelson Interferometry Summer School, Lowell Observatory, Flagstaff, AZ, May 21–25, 2001.
3. Lay, O.: Jet Propulsion Laboratory, Pasadena, CA. (Personal communication 2002–2003.)
4. Boden, A.: Elementary Theory of Interferometry. *Principles of Long Baseline Stellar Interferometry*, P. Lawson, ed., 1999, pp. 9–28.
5. Traub, W.: Beam Combination and Fringe Measurement. *Principles of Long Baseline Stellar Interferometry*, P. Lawson, ed., 1999, pp. 31–58.
6. Lay, O.: Separated Spacecraft Interferometry. Presentation given at the 2002 Michelson Interferometry Summer School, Harvard-Smithsonian Center for Astrophysics, Cambridge, MA, June 24–28, 2002.
7. Mackay, C. D.; Tubbs, R. N.; Bell, R.; Burt, D.; and Moody, I.: Sub-Electron Read Noise at MHz Pixel Rates. SPIE 4306 Conference Proceedings, Jan. 2001, pp. 289–298.
8. Rowe, B. H.: Astronomical Computing. *Sky & Telescope*, R. W. Sinnott, ed., June 1993, pp. 83–85.